Polymer Testing 124 (2023) 108082

Contents lists available at ScienceDirect

Polymer Testing

journal homepage: www.elsevier.com/locate/polytest

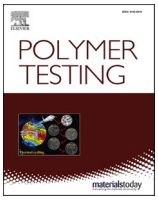

The micro response mechanisms of foamed polymer rehabilitation material under compression: From a closed cell view

Yongshen Wu [a,b,c,d], Chao Zhang [a,b,c,d,**], Cuixia Wang [a,b,c,d,*], Timon Rabczuk [e], Pengjia Zhu [f], Peng Zhao [a,g], Lei Wang [a,h], Xiaoying Zhuang [i], Juan Zhang [j], Hongyuan Fang [a,b,c,d]

[a] Yellow River Laboratory/Underground Engineering Institute, Zhengzhou University, Zhengzhou, 450001, China
[b] School of Water Conservancy and Civil Engineering, Zhengzhou University, Zhengzhou, 450001, China
[c] National Local Joint Engineering Laboratory of Major Infrastructure Testing and Rehabilitation Technology, Zhengzhou, 450001, China
[d] Collaborative Innovation Center for Disaster Prevention and Control of Underground Engineering Jointly Built By Provinces and Ministries, Zhengzhou, 450001, China
[e] Institute of Structural Mechanics, Bahaus University Weimar, Weimar, 99423, Germany
[f] The Fifth Engineering CO., LTD of China Railway Seventh Group, Zhengzhou, 450016, China
[g] Southern Institute of Infrastructure Testing and Rehabilitation Technology, Huizhou, 516029, China
[h] Wanhua Energysav Science & Technology Group CO., LTD, Yantai, 264006, China
[i] PhoenixD Excellence Cluster, Faculty of Mathematics and Physics, Leibniz University Hannover, Hannover, 30168, Germany
[j] China Communications Construction Group CO., LTD, Beijing, 100032, China

ARTICLE INFO

Keywords:
Molecular dynamics
Polyurethane cell
Deformation mechanisms
Micromechanical properties

ABSTRACT

Non-aqueous reactive foamed polyurethanes are widely used in the non-excavation rehabilitation of infrastructures and fundamental engineering. However, the effect of a microscopic cell on the understanding of micro-mechanical properties of a polyurethane is not clearly stated. In this work, a molecular model of a polyurethane closed cell is established corresponding to the field emission scanning electron microscopy results. Molecular dynamics simulations were subsequently employed to investigate the effect of a closed cell on the micro-mechanical response of polyurethane during compression. Based on the layered non-affine displacement and internal structure variables, we find that the existence of cells reduces changes in the polymer chain structure, i.e., the bond stretching, bond angle bending, and dihedral angle rotation. This makes slippage of the polymer chain more violent, and the farther away from the centre of the cell, the greater the level of the polymer chain slippage. In other words, chain slippage plays a key role in reducing the mechanical properties of a polymer. What' s more, it is found that the number of hydrogen bonds in the cell is significantly less than that in the elastomer, which also could reduce the mechanical properties of foamed polyurethane. This study provides an efficient route for studying the micro-mechanical characterization of foamed polyurethane.

1. Introduction

Non-aqueous reactive foamed polyurethane (PU) grout materials are extensively used in freeways [1], urban road [2], airport runways [3], ground reinforcement [4], and anti-seepage in dams [5] because of their advantages in short reaction time [6], high early strength [4], good impermeability [7], and fast-setting [8]. No matter where PU grout materials are used, they bear a compressive load and very often repeated compressive loads. Therefore, compressive mechanical properties are a dominant feature of PU grout materials in achieving a desirable grouting effect.

In recent years, there has been growing interest in the compressive mechanical properties of PU grout materials. It has been reported that the mechanical properties of PU grout materials are sensitive to temperature [9–11], strain rate [12–16], density [12,13,17], and cell growth direction [18,19]. This is affected by many factors, such as the polymer matrix, cell structure, cell distribution, etc. Many experimental results have shown that the foamed polymers will undergo four stages (linear elasticity, yield, stress plateau, and densification) during compression deformation [19]. At different deformation stages, the cell wall will display elastic bending, elastic stretching, and plastic bending successively [20,21]. It can be seen that the deformation of foamed

* Corresponding author. Yellow River Laboratory/Underground Engineering institute, Zhengzhou University, Zhengzhou, 450001, China.
** Corresponding author. Yellow River Laboratory/Underground Engineering institute, Zhengzhou University, Zhengzhou, 450001, China.
E-mail addresses: chao.zhang.zzu@outlook.com (C. Zhang), cuixia.wang@outlook.com (C. Wang).

https://doi.org/10.1016/j.polymertesting.2023.108082
Received 22 March 2023; Received in revised form 13 May 2023; Accepted 22 May 2023
Available online 25 May 2023

polymers is more complex than that of polymer elastomers. To elaborate on the intricate deformation mechanism of foamed polymers, numerous finite element analyses of the representative volume elements (RVEs) model was used to study the mechanical properties and deformation characteristics of polymer foams, including PU foams [22–24]. The results of these models explained the influence of cell size distribution, cell anisotropy, cell wall thickness and mass distribution between supports on the mechanical properties of foamed polymers commendably. For example, C. Barbier et al. [25] studied the influence of the relative density and irregularity of Voronoi closed-cell structures on their elastic characteristics and plastic characteristics. N.J.Mills et al. [22] found that elastic buckling would occur before pore yielded. This accumulation of elastic buckling is also the reason why the stress-strain curve before yielding changed from linear to nonlinear. They also found that a plastic hinge will form on the wall of the cells after the cells reach the yield strain, and then the cell walls will rotate around the plastic hinge until the cell walls contact each other. However, due to the limitation of simulation size, finite element simulation cannot directly provide the change process of polymer cells at the micro-scale. Therefore, it is necessary to study the mechanical properties of foamed polymers at the molecular scale.

Molecular dynamics (MD) simulations can obtain the trajectory and velocity information of particles in the simulation system and explain the mechanical response of materials from the atomic scale, which is a powerful supplement to theory and experimental methods. In recent years, MD simulations has been widely used in the study of polymers [26,27], and it has been proven that it can explain the compression and tensile mechanical properties of polymers well from the perspective of the motion of atoms and molecular chains. D. Hossain et al. [28] carried out a tensile simulation of polyethylene and found that with the increase of strain, the proportion of trans dihedral angles increased under different chain lengths and strain rates, which showed that the structure of the polyethylene chain changed with the deformation of the system. Rutledge et al. [29–35] published a series of papers dealing with MD modelling of the yielding of polyethylene and PU. They found that the stress-strain relationship and yield properties of these polymers also have obvious strain rate sensitivity, which is consistent with the experimental results. They found that the yield of polymers will be accompanied by local cavitation, chain slip extraction, partial melting, shear band formation, block slip, and other phenomena, which indicates that when deformation occurs, the structure of the polymer chain and the phase shift between polymer chains will occur simultaneously in the polymers. However, unlike actual foamed PU, these models are dense and have no internal cells. Also, it is still not known whether the motion of a polymer chain in the cell wall is different from that of polymer elastomers during compression deformation. Matthew D. Lane et al. [36–38] constructed a cell and elastomer model of a poly-4-methyl-1-pentene (PMP) material and studied the response of the elastomer and PMP cell to a shock wave. They found that the response in the cell was significantly different from that in the elastomer, which indicates that the existence of cells has a great impact on the properties of the polymers. Although they built a cell model, the model is connected, and it is not applicable to PU grouting materials with a closed cell structure. Therefore, it is necessary to build a molecular model of a PU closed cell and compare the motion of the polymer chain in the cell wall and polymer elastomers when the system is deformed.

Therefore, we prepared PU samples, investigated the microscopic morphology of PU using a field emission scanning electron microscope (FESEM), determined the distribution of cell diameters, and measured cell wall thickness. Combined with the results of the FESEM, a microscopic model of a PU closed cell with a density of 0.347 g/cm^3 and a PU elastomer model were constructed. Then, we compared the stress, layered non-affine displacement, hydrogen bonds, and internal structure variables (bond length, bond angle, dihedral angle distribution, and potential energy) between the PU closed cell and elastomer during compression deformation and studied the effect of cell on the molecular deformation mechanism of PU during compression deformation.

2. Experimental and simulation method

2.1. Experimental method

Polyphenylmethane polyisocyanate (PAPI) and Sucrose polyether polyol (SPEPO) [8,39] were used to make the PU in this study. These two components can quickly react and expand to form foamed PU when injected into a mould, without requiring water for the reaction. The mixing ratio of PAPI and SPEPO was designed as 1:1 by weight, which falls within the typical range used in actual grouting projects. The density of the specimen is controlled by controlling the amount of PAPI and SPEPO injected into the mould. Then the samples were left at room temperature for 24 h before demoulding, as depicted in Fig. 1a. Subsequently, the specimen could be demoulded, resulting in a sample density of 0.31 g/cm^3, which has been used in many experiments to study the mechanical properties of foamed PU [9,11,40].

To eliminate the influence of the external dense layer on the sample, the central portion of the sample was extracted and used for FESEM experimentation, as shown in Fig. 1b. Then, the samples were cut into thin slices with a thickness of about 10 mm and a layer of gold that is 2 mm thick was coated on the surface of the slices to increase the conductivity and improve the clarity and resolution of the image. The accelerating voltage and amplification factors of FESEM were set to 15.0 kV and 200–200000, respectively. Subsequently, the micromorphology of the sample was tested.

2.2. Simulation method

2.2.1. Model construction and simulation details

In this work, the long-chain PU model was constructed in Materials Studio (MS) [41]. The size of the initial model of the long-chain PU was 5.06 × 5.06 × 5.06 nm^3, including 9 PU chains with a total of 66,339 atoms. The MD simulations were carried out using the publicly package of LAMMPS [42], where OVITO was used for visualisation [43].

The optimized potentials for liquid simulations of all atoms (OPLS-AA) force field [44] was used to describe the interaction between atoms. The standard Newton equations of motion were integrated in time using the velocity verlet algorithm with a time step of 0.5 *fs*. The Particle-Particle Particle-Mesh (PPPM) method [45] was used to solve the long-range force with a real-space cut-off of 1.2 nm [29].

The simulations were performed as follows. First, the system was thermalised to 600 K with the NVT (i.e., constant particle number N, constant volume V, and constant temperature T) ensemble for 250 ps. Second, the structure was relaxed to a constant temperature using the NPT (i.e., constant particle number N, constant pressure P, and constant

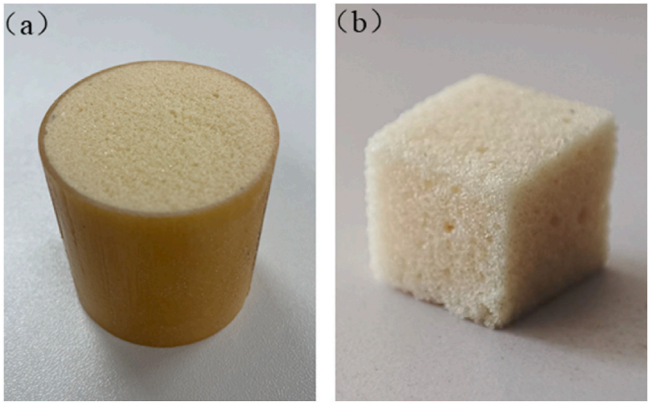

Fig. 1. Photograph of PU samples (a) with dense layer and (b) without dense layer.

temperature T) ensemble for 250 ps. The Nose-Hoover thermostat [46,47] was used to control the constant pressure and temperature. Third, the next relaxation cooled the structure down to 300 K for 300 ps (cooling rate of 1.0 K/ps), followed by further relaxation of 250 ps at 300 K. Fig. 2 presents a photograph of the PU elastomer.

After grouting, PU expands rapidly under the action of gas generated by the reaction between the foaming agent and raw materials to form the PU closed cells. In the process of expansion, the cell will also be constrained by the polymer matrix around the cell, and the resulting PU is composed of closed cells. In order to build the molecular model of a PU closed cells, we introduced two cells into the elastomer, which are marked as inner cell and outer cell. The inner cell can reflect the expansion process of PU, and the size of the inner cell gradually increases from 0 with an expansion rate of 0.1 nm/ns. The outer cell can reflect the restriction of the cell during expansion. Our construction methods for the molecular model of PU closed cells have been previously reported [39]. Fig. 3 is a cross-sectional view of the cell; its density is 0.347 g/cm^3. The outer diameter and inner diameter of the cell is 7.5 nm and 5.9 nm, respectively, and the thickness of the cell wall is 1.6 nm. In Fig. 3, the colour gradient of the wall atoms represents the position distribution of the atoms along the X direction.

2.2.2. Compression simulation

The PU elastomer and PU closed cell were then deformed under a uniaxial compress strain applied at a constant strain rate of 1×10^{10} s^{-1} with a zero-pressure condition for the two lateral simulation cell faces. Computation costs have restricted the lower limit of feasible strain rates in this study, owing to our use of an all-atom model. The ultra-low strain rate employed in the experiment surpasses the limits of current computational resources. Therefore, we referred to the strain rate of polymer MD simulations in the literature [48]. During the simulation, the ensemble is NPT, and the temperature was controlled to be 300 K. Nine different initial configurations were selected for each model, and the average stress calculated from the nine different configurations was used as the stress value of the system under different conditions.

3. Results and discussion

3.1. Micromorphology

Fig. 4a shows the representative micromorphology of the PU with a density of 0.31 g/cm^3. In the FESEM image, the white areas represent cell walls, while the grey or black parts indicate blank regions within the cells. It can be seen that PU can be considered a kind of matrix made of numerous hollow cells. To measure the cell size, the FESEM image was depicted by Photoshop (PS), as shown in Fig. 4b. After that, the pixel value of the cell can be obtained using the lasso tool in PS, and then the cross-section area (S) of each cell can be converted based on the pixel

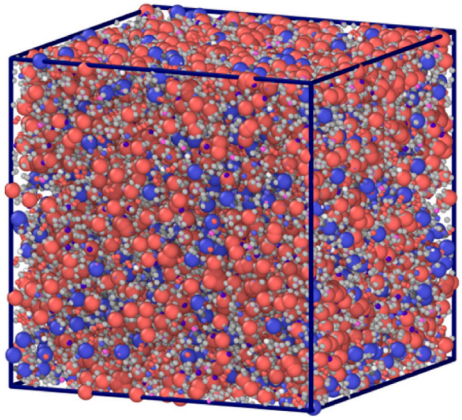

Fig. 2. Molecular model of PU elastomer.

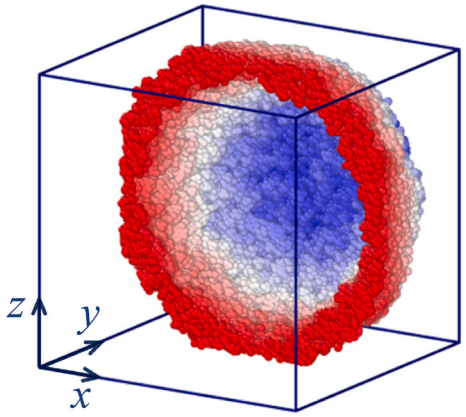

Fig. 3. The cross-sectional view of a PU closed cell.

value of the unit area [8,49]. According to the cross-section area of the cell, the equivalent diameter (De) of the cells can be calculated using Eq. (1), and then the distribution of De can be calculated as shown in Fig. 6a. Meanwhile, Fig. 5 shows the FESEM image of the cell walls, magnified by factors of 50,000 and 200,000, respectively. In PS, the cell wall thickness is also expressed in pixels and then converted to the actual length unit (μm) using the ruler's tool. We measured the thickness of several cell walls in the image and plotted the distribution of cell wall thickness in Fig. 6b.

According to the distribution of cell diameter and cell wall thickness, the average cell diameter is 136.41 μm. The average value of cell wall thickness is 0.1891 μm. The ratio of the average diameter of the cells to the average thickness of the cell walls is 721.35. It can be seen that the cell diameter is far greater than the thickness of the cell wall, so it can be known that the cell is a thin-walled hollow elastic structure, similar to the thin-walled hollow elastic sphere mentioned in the literature [50,51]. There are examples in the literature [51] of plate compression experiments and simulations on thin-walled hollow elastic spheres, and the method for calculating the reduced force is shown in Eq. (2). It is known that the ratio of the cell diameter to the cell wall thickness will affect the mechanical characteristics of a thin-walled hollow cell. Because the cell diameter is much larger than the cell wall thickness, the cell wall will have more complex deformation than the polymer elastomer or the polymer matrix filled between the cells. This will lead to a different motion of polymer chains in the cell wall from that of the polymer elastomer or polymer matrix filled between cells during compression deformation. This will be discussed in the following sections.

$$De = \sqrt{\frac{4S}{\pi}} \tag{1}$$

$$\frac{R}{Eh^3}F = \begin{cases} \frac{3}{8}C_0(\nu)\varepsilon^{1/2} + 3C_1(\nu)\varepsilon^2 \\ \frac{3}{2}C_0(\nu)\varepsilon^{1/2} + C_2(\nu) \end{cases} \tag{2}$$

$$\varepsilon = x/h \tag{3}$$

Where R is the cell radius; E is the elastic modulus; h is the cell wall thickness; ν is the Poisson's ratio; C_0, C_1, C_2 are dimensionless parameters; and ε is the dimensionless displacement. The calculation formula of ε is shown in Eq. (3), where x is the displacement of the cell wall being compressed.

3.2. Stress-strain behaviour

Fig. 7 shows the stress-strain relationship of a PU elastomer and a PU

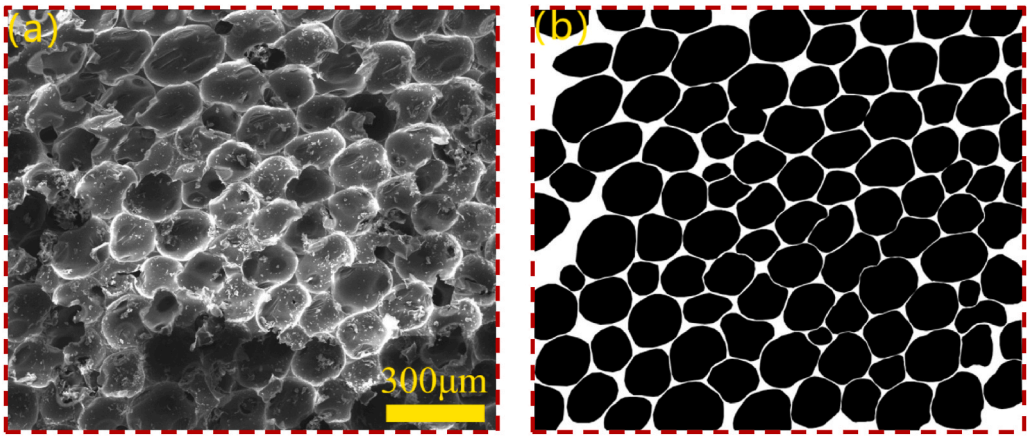

Fig. 4. Comparison between (a) the original FESEM image and (b) the binary image of PU.

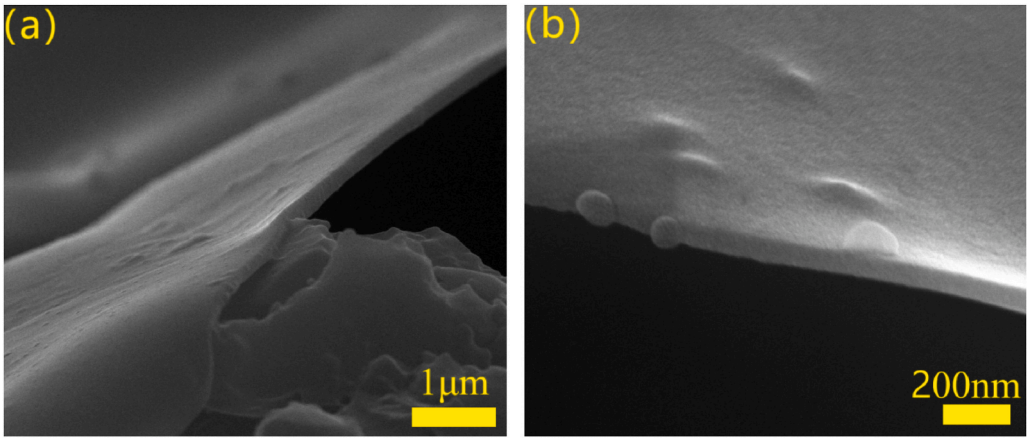

Fig. 5. FESEM images of the wall of PU samples with a magnification factor of (a) 50,000 and (b) 200,000.

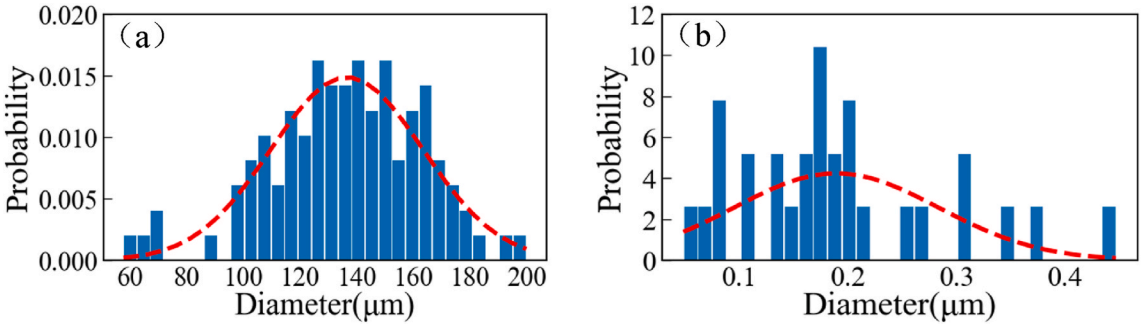

Fig. 6. Probability distribution of (a) the diameter and (b) the wall thickness of cells in PU.

closed cell, which is compared with the stress-strain results obtained from experiments in the literature [9,55], where the density of foamed PU in the literature [9] is 0.31 g/cm^3. It can be seen that the stress-strain curve obtained by our simulation is consistent with the experimental results, whether it is the PU elastomer or PU closed cell. There are four distinct regimes: linear elasticity, yield, softening, and hardening. Similar behaviours were also reported in other MD compression simulations [35]. According to the experimental results, shown in Fig. 7, the stress of the polymers will increase significantly with an increase in strain rate, and the strain rate simulated in this paper is 1×10^{10} s^{-1}, which is far greater than the strain rate of the experiment in the literature, so under the same strain, the stress obtained in this paper is greater than the stress obtained in the experiment. With the use of suitable extrapolation method, molecular simulation results can be extrapolated to the strain rate of experiments [52]. This is not the focus of this paper and the quantitative analysis of the microscopic mechanical properties of foamed PU using this method will be conducted in the future.

3.3. Hydrogen bonds

As a physical crosslinking point, hydrogen bonds (H-bonds) can limit the movement of polymer chains and further improve the mechanical properties of polymers. In this paper, geometric criteria was used to determine the formation of H-bonds, demonstrated in Fig. 8a. When the distance (d) between the donor (D) and acceptor (A) is less than 3.5 Å and the angle (α) between D-H and D-A is less than 30°, H-bonds will be

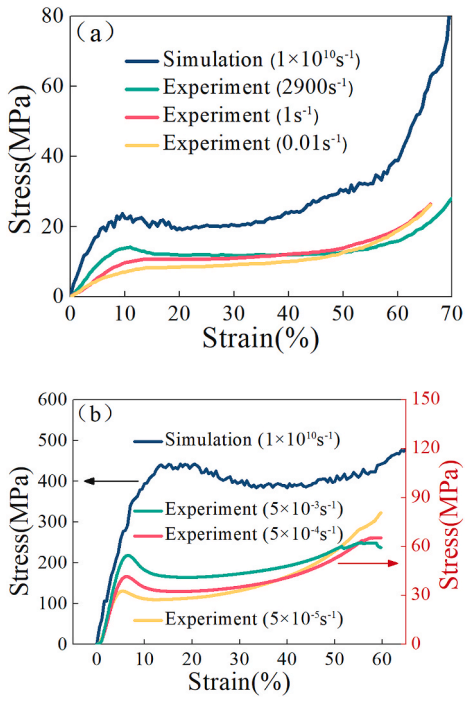

Fig. 7. Stress-strain response of (a) the PU closed cell and (b) PU elastomer deformed in uniaxial compression at strain rate of 10^{10} s^{-1} and temperature of 300 K.

formed. In the PU, there are 9 kinds of H-bonds that can be formed, as shown in Fig. 8b. When the strain is 0, the number of different types of H-bonds in the PU closed cell and PU elastomer is shown in Fig. 9a. It can be seen that the H-bonds formed in the PU closed cell and PU elastomer are mainly the H-bonds formed with the participation of hydroxyl groups, accounting for 83.57% and 81.16% of the total H-bonds, respectively. Fig. 9b shows the relationship between the number of H-bonds and the strain. It can be seen that the number of H-bonds in the PU elastomer are significantly more than those in the PU closed cell. Although the number of H-bonds in the elastomer decreases suddenly when the strain is greater than 35%, the number of H-bonds in the PU closed cell is still less than that in the PU elastomer. With the increase of strain, the number of H-bonds in the cell increases slightly because the cell wall at the edge of the cell contact with each other, which increases the possibility of H-bonds formation. The results of the experiment and simulation show that the stress of the PU elastomer is significantly greater than that of the PU closed cell, as shown in Fig. 7. In addition to the influence of the thin-walled hollow structure on the mechanical properties of the cell, the reduction in the number of H-bonds is also one of the reasons for the reduction of its mechanical properties.

3.4. *Layered non-affine displacement*

The atomic displacement of a polymer during deformation consists of two parts, one is due to the box deformation, and the other is due to the slippage of polymer chain. Non-affine displacement can be used to represent the level of the slippage of polymer chain. The method of overall non-affine displacement (U) has been previously reported [39]. In Fig. 10, we report the variation of U with the axial strains. It can be

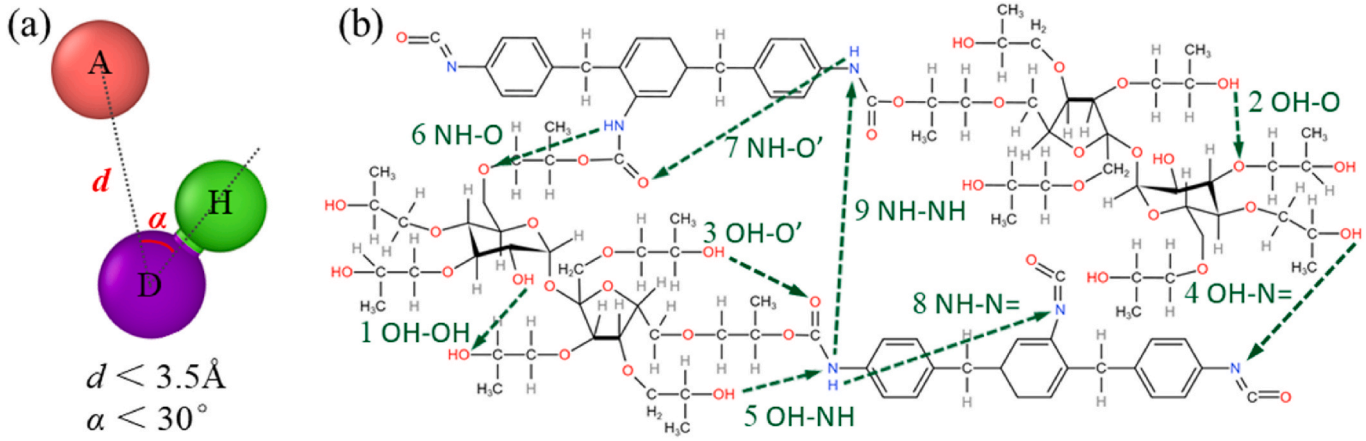

Fig. 8. (a) Geometric criteria for H-bonds. D is the donor, and A is the acceptor, (b) Schematic diagram of several types of H-bonds in PU.

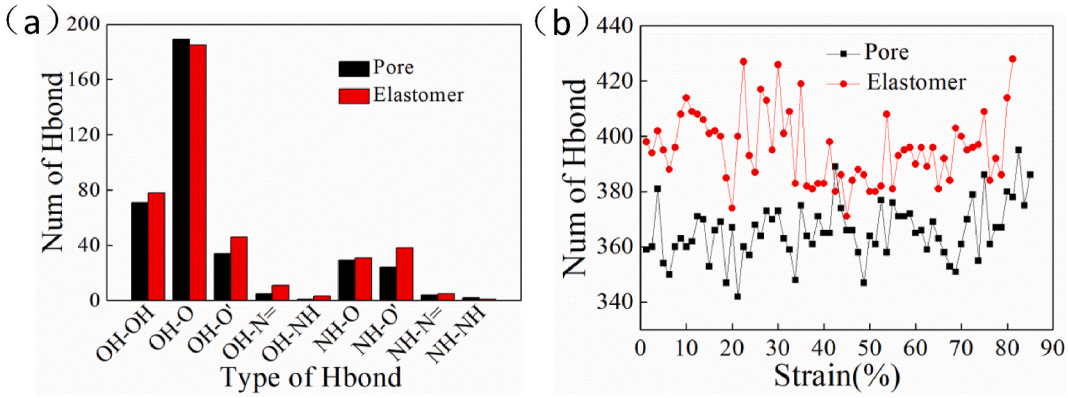

Fig. 9. (a) Number of H-bonds per type, (b) The total number of H-bonds in PU as a function of strain.

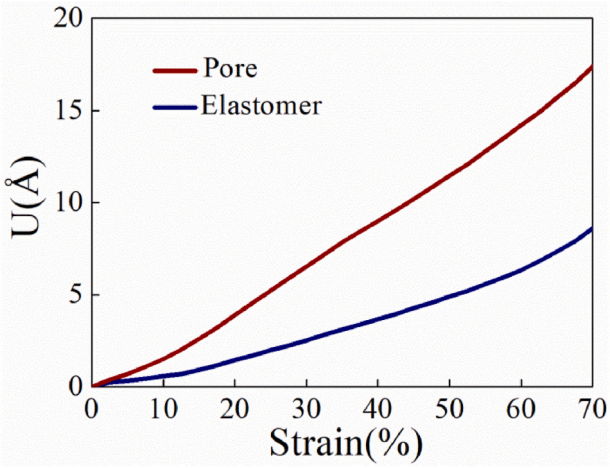

Fig. 10. Non-affine displacement of the PU elastomer and PU closed cell.

seen that the value of U in the PU closed cell is significantly greater than that in the PU elastomer, and the greater the strain, the more obvious the phenomenon. This shows that the existence of cell makes the polymer chain slips more violently.

In order to better explain the effect of the cell on PU, we divide the PU closed cell and PU elastomer into the same number of layers, and each layer contains the same number of atoms, as shown in Fig. 11. The average non-affine displacements of atoms in each layer are shown in Figs. 12 and 13. The results show that the average non-affine displacement of the atoms in each layer of the PU closed cell is related to the distance from the atom to the centre of the cell. The farther away from the centre of the cell, the greater the average non-affine displacement of the layer of atoms, and the greater the strain, the more obvious the phenomenon. This is affected by the curvature of the cell wall. The farther away from the centre of the cell, the greater the deformation of the cell wall and the more obvious slippage of the polymer chain. With the increase of strain, the inner cell walls will gradually contact and fuse, so the greater the strain, the greater the difference between the average non-affine displacement of the inner and outer atoms. However, the

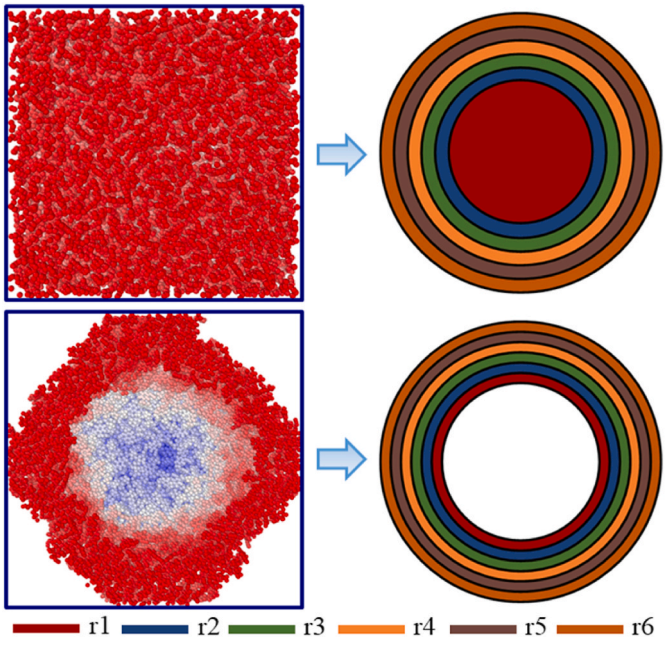

Fig. 11. Illustration of atomic layers with the thickness from the centre of the model.

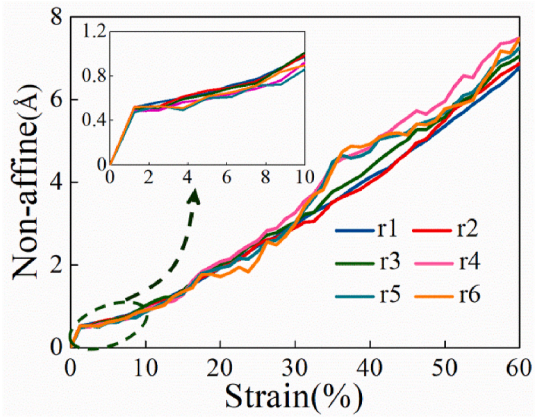

Fig. 12. Layered non-affine of the PU elastomer.

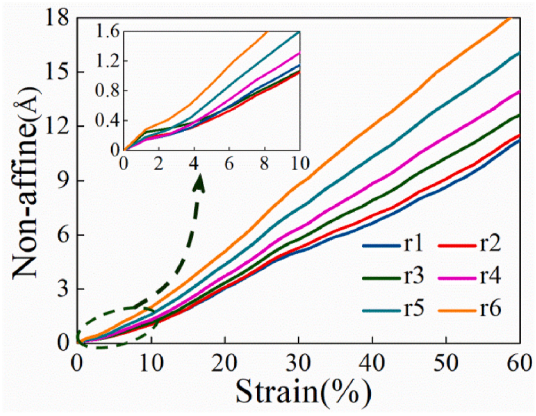

Fig. 13. Layered non-affine of the PU closed cell.

average non-affine displacement of the atoms in each layer of PU elastomer is almost the same, which indicates that the level of slippage of the polymer chain in each layer of the PU elastomer is very close.

3.5. Evolution of internal structure variables

3.5.1. Bond length and bond angle evolution

The change of bond length and bond angle with strain can provide a reference for understanding the deformation of polymer structure. Figs. 14 and 15 show the change in average bond length and average bond angle with strain in a PU closed cell and PU elastomer. It can be seen that with the increase of the strain, the average bond length of the PU elastomer gradually increases, and the average bond angle of the PU

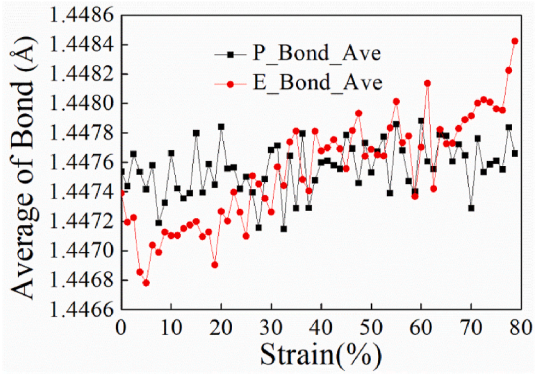

Fig. 14. Average bond length as a function of strain.

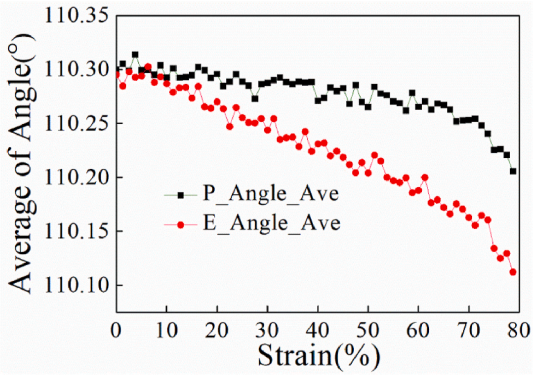

Fig. 15. Average bond angle as a function of strain.

elastomer gradually decreases. However, the average bond length of the PU closed cell does not change significantly with strain. Although the average bond angle of the PU closed cell decreases gradually with the increase of strain, the decrease rate of the average bond angle of the PU closed cell is still significantly lower than that of the PU elastomer. This shows that the polymer chain structure in the PU elastomer has a greater change than that in the PU closed cell. However, the results of non-affine displacement show that under the same conditions, the average non-affine displacement of atoms in the PU closed cell is significantly greater than that in the PU elastomer; that is, the atoms in the PU closed cell are moving more violently. Therefore, we can know that the existence of the cell will reduce the level of structural change of the polymer chain and cause more chain segment slippage.

3.5.2. *Dihedral conformation evolution*

The dihedral angle is usually used to characterise the conformation of a polymer chain [53]. As shown in Fig. 16, when the turning angle points outward, φ is positive. When the turning angle points inward, φ is negative. The value range of φ is −180°–180°. When the angle, φ is $-60° \leq \varphi \leq 60°$, it is a trans dihedral angle (trans); when $-180° \leq \varphi \leq -60°$ or $60° \leq \varphi \leq 180°$, it is a gauche dihedral angle (gauche). Generally, the lowest energy point of the trans dihedral angle is about 0°, the lowest energy point of a gauche dihedral angle is about −120° or 120°, and the lowest energy of a trans dihedral angle is less than the gauche dihedral angle, so the trans dihedral angle is more stable, and the conversion of the gauche dihedral angle to a trans dihedral angle needs to overcome a large energy barrier [54]. Fig. 17 shows the dihedral angle distribution when the strain is 0. It can be seen that when the strain is 0%, the dihedral angle distribution of the PU closed cell and the PU elastomer are basically the same, which indicates that the existence of the cell will not affect the initial configuration of the dihedral angle. Fig. 18 shows how the percent of the trans conformations evolves as a function of strain. It can be seen that the percentage of trans conformations in the PU elastomer fluctuates more with the increase of strain, especially in the range of 0%–20% strain. This shows that the conversion of the dihedral angle in the PU elastomer between the trans conformations and the gauche conformations is more frequent than that in the PU closed cell. The existence of the cell can inhibit the rotation of the polymer chain at the initial stage of deformation to a certain extent, which is

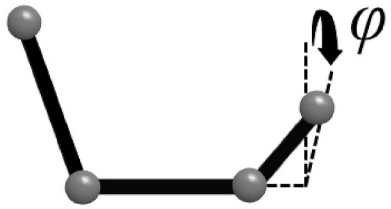

Fig. 16. The diagram of dihedral angle.

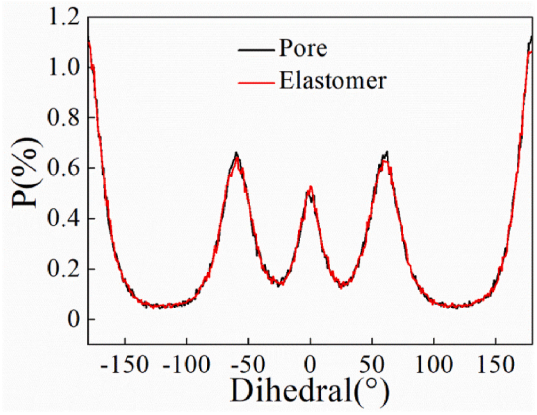

Fig. 17. The dihedral angle distribution of the PU closed cell and PU elastomer with a strain of 0%.

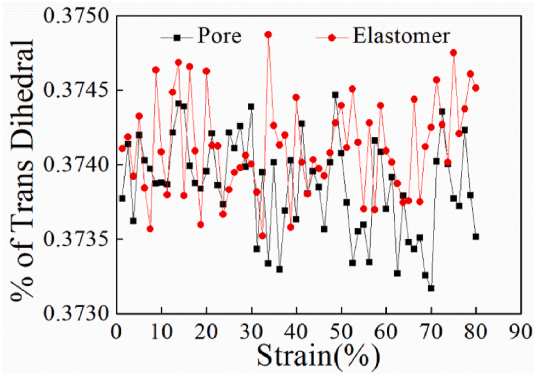

Fig. 18. Chain dihedral angle evolution as a function of strain.

consistent with the previous results of the relationship between the bond length and the bond angle with strain.

3.5.3. *Internal energy evolution*

Figs. 19 and 20 illustrate the potential energy change of the PU closed cell and PU elastomer, respectively. In addition to the total energy, E_{total}, the individual components of the energy are shown: the non-bonded energy E_{pair}, the bonding energy E_{bond}, the bond angle energy E_{angle}, and the dihedral angle energy $E_{dihedral}$. In the PU elastomer, when the strain is less than 25%, the non-bonded energy increases sharply with an increase in strain from 0% to 25%. Unlike the non-bonded energy, the bond angle energy and dihedral angle energy increase slowly with an increase in strain. We can know that the total energy sharply

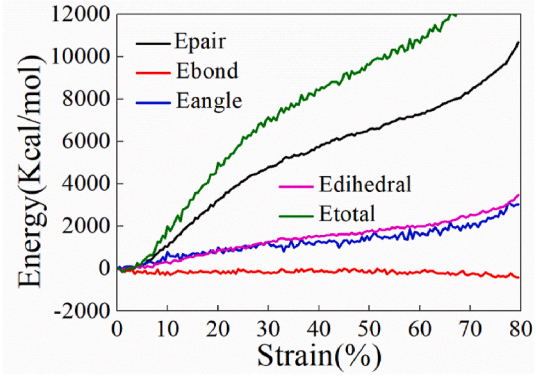

Fig. 19. Energy decomposition for the PU elastomer.

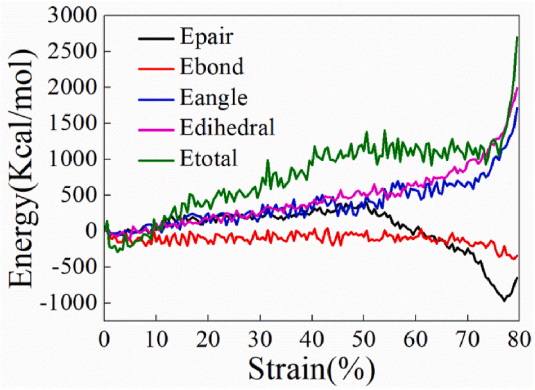

Fig. 20. Energy decomposition for the PU closed cell.

increases in the PU elastomer due to non-bonded interactions when strain is less than 25%. This indicates that the main changes in a polymer chain in a PU elastomer at this stage are changes in polymer chain structure, such as bond angle bending and dihedral angle rotation. When the strain reaches about 25%, the rate of non-bonded interaction energy increase begins to decrease, which can be associated with chain slippage mechanisms. This indicates that the polymer chain obviously begins to slip in the PU elastomer at this time. It is worth mentioning that although the increasing rate of non-bonded interaction energy decreases, it is still significantly greater than the increasing rate of bond angle energy and dihedral angle energy. This shows that the changes in polymer chain structure are continuing while the polymer chain slip occurs. In the PU closed cell, with the increase of strain, the non-bonded interaction energy is less than the bond angle energy and dihedral angle energy. Notably, when the strain reaches about 0.5, the non-bonded interaction energy of the cell decreases suddenly, the bond angle energy and the dihedral angle energy continue to increase, and the bonded energy remains almost unchanged. This indicates that the bond angle energy and dihedral angle energy play a significant role in the change of total energy of a PU closed cell, which indicates that the molecular chain slippage of the PU closed cell is more obvious than that of the PU elastomer. Combined with the results of bond length, bond angle, and dihedral angle distribution, it can be concluded that when the strain is small, the chain structure changes mainly in the PU elastomer, such as chain expansion and dihedral angle rotation, and the chain slippage will increase with the increase of strain. Compared with a PU elastomer, the level of change in the polymer chain structure in a PU closed cell is relatively low. Instead, the cell will have obvious intermolecular chain slippage even if the strain is small, so the cell will yield and fail under a smaller strain.

4. Conclusion

In this paper, the micromorphology of a foamed PU with a density of 0.31 g/cm^3 was observed, and the distribution of cell diameter and cell wall thickness were determined. Based on the results of FESEM, the molecular model of a PU closed cell with a density of 0.347 g/cm^3 was constructed, and the effect of the cell on the molecular deformation mechanism during compression deformation was studied systematically. The conclusions drawn are as follows:

(1) A foamed PU is composed of closed cells packed together, with an average cell diameter of 136.41 μm. The average value of cell wall thickness is 0.1891 μm. The ratio of the average cell diameter to the average cell wall thickness is 721.35. It's worth noting that the cell diameter is significantly larger than the cell wall thickness. The FESEM results show that the cells in a PU are thin-walled hollow structures.

(2) The average non-affine displacement of atoms in a PU closed cell is significantly greater than that in a PU elastomer, indicating that the movement of atoms in the cell is more intense. Furthermore, there is a noticeable layering phenomenon observed in the movement of atoms within the cell walls. The farther away from the centre of the cell, the greater the non-affine displacement of atoms, and the more intense the movement of atoms. However, no such layering phenomenon was found in the PU elastomer.

(3) The present simulations clearly show that the level of bond stretching, bond angle bending, and dihedral angle rotation of a PU closed cell is significantly weaker than that of a PU elastomer. Also, the energy evolution plots show that non-bonded interactions played a significant role in the total potential energy of the PU elastomer, while bond angle energy and dihedral angle energy play a significant role in the total potential energy changes of the PU closed cell. This indicates that the existence of cells reduces the changes in polymer chain structure, resulting in more inter-chain slippage motion of the polymer chain. Additionally, the total number of H-bonds in the PU elastomer is significantly greater than in the PU closed cell. Thus, the stress of a PU closed cell is much lower than that of a PU elastomer.

Author statement

Yongshen Wu: Methodology, Investigation, Data Curation, Writing - Original Draft.

Chao Zhang: Funding acquisition, Methodology, Writing- Original Draft.

Cuixia Wang: Investigation, Supervision, Review & Editing, Revision.

Timon Rabczuk: Investigation, Data analysis, Revision.

Pengjia Zhu: Investigation, Data analysis.

Peng Zhao: Investigation, Data Curation, Editing Draft.

Lei Wang: Investigation, Data Curation, Editing Draft.

Xiaoying Zhuang: Investigation, Data Curation, Editing Draft.

Juan Zhang: Investigation, Data Curation, Editing Draft.

Hongyuan Fang: Funding acquisition, Data analysis, Writing-Original Draft.

Declaration of competing interest

The authors declare the following financial interests/personal relationships which may be considered as potential competing interests: James M. Carothers is an advisor to Wayfinder Biosciences.

Data availability

The authors do not have permission to share data.

Acknowledgment

This research was supported by the National Natural Science Foundation of China (No. 52178368, 51978630, 51909242, 52009125), the Program for Science and Technology Innovation Teams and Talents in Universities of Henan Province (No. 23IRTSTHN004 and 23HASTIT007), the Guangdong Innovative and Entrepreneurial Research Team Program (2016ZT06N340), the Program for Guangdong Introducing Innovative and Entrepreneurial Teams (NO. HG-GCKY-01-002), the China Postdoctoral Science Foundation (No. 2020TQ0285, 2022M722882), Key Project of Natural Science of Henan Province (232300421137), Central Plains Talent Program - Top Talents of Central Plains Youth, Research Preferential Foundation for Selected Overseas Chinese of Henan Province, the First-class Project Special Funding of Yellow River Laboratory (YRL22LT07), and Key scientific research projects of colleges and universities in Henan Province (No. 21A570007), for which the authors are grateful acknowledged.

References

[1] J. Li, J. Zhang, J. Xu, F. Wang, B. Wang, Q. Li, Dynamic behavior of polymer antiseepage wall for earth dam by centrifuge test, Int. J. GeoMech. 18 (12) (2018), 04018179: 1-04018179: 17.

[2] K. Liu, W. Liang, F. Ren, J. Ren, F. Wang, H. Ding, The study on compressive mechanical properties of rigid polyurethane grout materials with different densities, Construct. Build. Mater. 206 (2019) 270–278.

[3] S. Kazemian, B. Huat, Assessment and comparison of grouting and injection methods in geotechnical engineering, Eur. J. Sci. Res. 52 (1) (2009) 51–59.

[4] Z. Yang, X. Zhang, X. Liu, X. Guan, C. Zhang, Y. Niu, Flexible and stretchable polyurethane/waterglass grouting material, Construct. Build. Mater. 138 (2017) 240–246.

[5] C. Guo, F. Wang, Mechanism study on the construction of ultra-thin antiseepage wall by polymer injection, J. Mater. Civ. Eng. 24 (9) (2012) 1183–1192.

[6] Z. Lin, C. Guo, D. Cao, et al., An experimental study on the cutting failure of polymer grouting, Construct. Build. Mater. 258 (2020), 119582.

[7] J. Chen, X. Yin, H. Wang, Y. Ding, Evaluation of durability and functional performance of porous polyurethane mixture in porous pavement, J. Clean. Prod. 188 (2018) 12–19.

[8] M. Li, M. Du, F. Wang, B. Xue, C. Zhang, H. Fang, Study on the mechanical properties of polyurethane (PU) grouting material of different geometric sizes under uniaxial compression, Construct. Build. Mater. 259 (2020), 119797.

[9] B. Song, W. Lu, C. Syn, W. Chen, The effects of strain rate, density, and temperature on the mechanical properties of polymethylene diisocyanate (PMDI)-based rigid polyurethane foams during compression, J. Mater. Sci. 44 (2) (2009) 351–357.

[10] D.A. Apostol, D.M. Constantinescu, Temperature and speed of testing influence on the densification and recovery of polyurethane foams, Mech. Time-Dependent Mater. 17 (1) (2013) 111–136.

[11] M. Shi, F. Wang, J. Luo, Compressive strength of polymer grouting material at different temperatures, J. Wuhan Univ. Technol.-Materials Sci. Ed. 25 (6) (2010) 962–965.

[12] M. Kirpluks, U. Cabulis, J. Andersons, G. Japins, K. Kalnins, Modeling the effect of foam density and strain rate on the compressive response of polyurethane foams, SAE.Int. J. Mater. Manuf. 11 (2) (2018) 131–138.

[13] K.B. Bhagavathula, C.S. Meredith, S. Ouellet, S.S. Satapathy, D.L. Romanyk, J. D. Hogan, Density, microstructure, and strain-rate effects on the compressive response of polyurethane foams, Exp. Mech. 62 (3) (2021) 505–519.

[14] O. Weißenborn, C. Ebert, M. Gude, Modelling of the strain rate dependent deformation behaviour of rigid polyurethane foams, Polym. Test. 54 (2016) 145–149.

[15] S. Ouelleta, D. Croninb, M. Worswick, Compressive response of polymeric foams under quasi-static,medium and high strain rate conditions, Polym. Test. 25 (2006) 731–743.

[16] A. Pellegrino, V.L. Tagarielli, R. Gerlach, N. Petrinic, The mechanical response of a syntactic polyurethane foam at low and high rates of strain, Int. J. Impact Eng. 75 (2015) 214–221.

[17] F. Saint-Michel, L. Chazeau, J.-Y. Cavaillé, E. Chabert, Mechanical properties of high density polyurethane foams: I. Effect of the density, Compos. Sci. Technol. 66 (15) (2006) 2700–2708.

[18] Z.H. Tu, V.P.W. Shim, C.T. Lim, Plastic deformation modes in rigid polyurethane foam under static loading, Int. J. Solid Struct. 38 (2001) 9267–9279.

[19] M. Marvi-Mashhadi, C.S. Lopes, J. Llorca, High fidelity simulation of the mechanical behavior of closed-cell polyurethane foams, J. Mech. Phys. Solid. 135 (2020), 103814.

[20] M.C. Saha, H. Mahfuz, U.K. Chakravarty, M. Uddin, M.E. Kabir, S. Jeelani, Effect of density, microstructure, and strain rate on compression behavior of polymeric foams, Mater. Sci. Eng.A 406 (2005) 328–336.

[21] M. Avalle, G. Belingardi, R. Montanini, Characterization of polymeric structural foams under compressive impact loading by means of energy-absorption diagram, Int. J. Impact Eng. 25 (2001) 455–472.

[22] N.J. Mills, R. Stämpfli, F. Marone, P.A. Brühwiler, Finite element micromechanics model of impact compression of closed-cell polymer foams, Int. J. Solid Struct. 46 (2009) 677–697.

[23] M. Marvi-Mashhadi, C.S. Lopes, J. Llorca, Effect of anisotropy on the mechanical properties of polyurethane foams: an experimental and numerical study, Mech. Mater. 124 (2018) 143–154.

[24] M. Marvi-Mashhadi, C. Lopes, J. Llorca, Modelling of the mechanical behavior of polyurethane foams by means of micromechanical characterization and computational homogenization, Int. J. Solid Struct. 146 (2018) 154–166.

[25] C. Barbier, P.M. Michaud, D. Baillis, J. Randrianaliso, A. Combescure, New laws for the tension/compression properties of Voronoi closed-cell polymer foams in relation to their microstructure, Eur. J. Mech. Solid. 45 (2014) 110–122.

[26] Q. Bao, Z. Yang, Z. Lu, Molecular dynamics simulation of amorphous polyethylene (PE) under cyclic tensile-compressive loading below the glass transition temperature, Polymer 51 (2010) 6071–6083.

[27] K. Yashiroa, T. Itob, Y. Tomita, Molecular dynamics simulation of deformation behavior in amorphous polymer: nucleation of chain entanglements and network structure under uniaxial tension, Int. J. Mech. Sci. 45 (2003) 1863–1876.

[28] D. Hossain, M.A. Tschopp, D.K. Ward, J.L. Bouvard, P. Wang, M.F. Horstemeyer, Molecular dynamics simulations of deformation mechanisms of amorphous polyethylene, Polymer 51 (2010) 6071–6083.

[29] P.A.T. Olsson, P.J. in't Veld, E. Andreasson, E. Bergvall, E.P. Jutemar, V. Petersson, G.C. Rutledge, M. Kroon, All-atomic and coarse-grained molecular dynamics investigation of deformation in semi-crystalline lamellar polyethylene, Polymer 153 (2018) 305–316.

[30] N. Lempesis, P.J. in't Veld, G.C. Rutledge, Atomistic simulation of the structure and mechanics of a semicrystalline polyether, Macromolecules 49 (2016) 5714–5726.

[31] I.C. Yeh, J.L. Lenhart, G.C. Rutledge, Molecular dynamics simulation of the effects of layer thickness and chain tilt on tensile deformation mechanisms of semicrystalline polyethylene, Macromolecules 50 (4) (2017) 1700–1712.

[32] N. Lempesis, P.J. in't Veld, G.C. Rutledge, Atomistic simulation of a thermoplastic polyurethane and micromechanical modeling, Macromolecules 50 (2017) 7399–7409.

[33] N. Lempesis, P.J. in't Veld, G.C. Rutledge, Simulation of the structure and mechanics of crystalline 4,4′-diphenylmethane diisocyanate (MDI) with n-butanediol (BDO) as chain extender, Polymer 107 (2016) 233–239.

[34] S. Zhu, N. Lempesis, P.J. in't Veld, G.C. Rutledge, Molecular simulation of thermoplastic polyurethanes under large tensile deformation, Macromolecules 51 (5) (2018) 1850–1864.

[35] S. Zhu, N. Lempesis, P.J. in't Veld, G.C. Rutledge, Molecular simulation of thermoplastic polyurethanes under large compressive deformation, Macromolecules 51 (22) (2018) 9306–9316.

[36] J.M.D. Lane, G.S. Grest, T.R. Mattsson, Hot spot and temperature analysis of shocked hydrocarbon polymer foams using molecular dynamics simulation, Comput. Mater. Sci. 79 (2013) 873–876.

[37] T.R. Mattsson, J.M.D. Lane, K.R. Cochrane, M.P. Desjarlais, A.P. Thompson, F. Pierce, G.S. Grest, First-principles and classical molecular dynamics simulation of shocked polymers, Phys. Rev. B Condens. Matter 81 (5) (2010), 054103: 1-054103: 9.

[38] J.M.D. Lane, G.S. Grest, A.P. Thompson, K.R. Cochrane, M.P. Desjarlais, T. R. Mattsson, Shock compression of hydrocarbon polymer foam using molecular dynamics, AIP Conf. Proc. 1426 (1) (2012).

[39] Y. Wu, C. Zhang, C. Wang, J. Wan, N. Wei, C. Zhu, H. Fang, Z. Zou, Micro-mechanical properties of foamed polymer rehabilitation material: a molecular dynamics study, Polymer 263 (2022), 125480.

[40] W. Pan, C. Zhang, C. Wang, H. Fang, F. Wang, Z. Qin, J. Zhang, L. Wang, Compressive fatigue resistance and related microscopic mechanisms in foamed polyurethane grouting materials for roadbed rehabilitation, Int. J. Fatig. 171 (2023), 107593.

[41] San Diego, CA, USA, Accelrys. Materials Studio Release vol. 6.0, 2011.

[42] LAMMPS (Large-scale Atomic/Molecular Massively Parallel Simulator), open source code, http://www.cs.sandia.gov/wsjplimp/la mmps.html.

[43] A. Stukowski, Visualization and analysis of atomistic simulation data with OVITO-the open visualization Tool modelling, Model. Simulat. Mater. Sci. Eng. 18 (2010), 015012.

[44] W.L. Jorgensen, D.S. Maxwell, J. TiradoRives, Development and testing of the OPLS all-atom force field on conformational energetics and properties of organic liquids, J. Am. Chem. Soc. 118 (45) (1996) 11225–11236.

[45] R.W. Hockney, J.W. Eastwood, Computer Simulation Using Particles, CRC Press, Bristol, 1998.

[46] W.G. Hoover, Phys Rev A, vol. 31, 1985, p. 1695.

[47] W.G. Hoover, Phys Rev A, vol. 34, 1986, p. 2499.

[48] A.L. Bowman, S. Mun, B.D. Huddleston, S.R. Gwaltney, M.I. Baskes, M. F. Horstemeyer, A nanoscale study of size scale, strain rate, temperature, and stress state effects on damage and fracture of polyethylene, Mech. Mater. 161 (2021), 104008.

[49] S. Chen, Y. Tian, C. Li, W. Duan, A new scheme for analysis of pore characteristics using centrifuge driven non-toxic metal intrusion, Geomech. Geophys. Geo-Energy Geo-Resour 2 (3) (2016) 173–182.

[50] Z. Yousaf, M. Smith, P. Potluri, W. Parnell, Compression properties of polymeric syntactic foam composites under cyclic loading, Composites Part B 186 (2020), 107764.

[51] S. Robert, D.S. John, A.C. Vincent, J.C.B. James, Axial compression of hollow elastic spheres, J. Mech. Mater. Struct. 5 (2010) 693–705.

[52] D.Ö. Hüsamettin, N. Fritjof, T.O. Richard, S.H. Mikael, Prediction of real tensile properties using extrapolations from atomistic simulations; an assessment on thermoplastic starch, Polymer 228 (2021), 123919.

[53] S. Yang, J. Qu, Computing thermomechanical properties of crosslinked epoxy by molecular dynamic simulations, Polymer 53 (2012) 4806–4817.

[54] C. Wu, W. Xu, Atomistic molecular simulations of structure and dynamics of crosslinked ,epoxy resin, Polymer 48 (2007) 5802–5812.

[55] Hongyuan Fang, Peng Zhao, Chao Zhang, Pan Wang, Zisen Yu, Kun Cai, Cuixia Wang, Juan Wang, Mingrui Du, Wei He, Ruitao Zhao, Deng Nan, A cleaner polyurethane elastomer grouting material with high hardeningstrain for the fundamental rehabilitation: The comprehensive mechanicalproperties study, Construct. Build. Mater. 318 (2022) 125951.